PNAS RESEARCH ARTICLE | EARTH, ATMOSPHERIC, AND PLANETARY SCIENCES

Miocene and Pliocene ice and air from the Allan Hills blue ice area, East Antarctica

S. Shackleton[a,b,1,2], V. Hishamunda[a], L. Davidge[c], E. Brook[d], J. Marks Peterson[d], A. Carter[e], S. Aarons[e], A. Kurbatov[f], D. Introne[f], Y. Yan[g], I. M. Nesbitt[f], C. Buizert[d], E. J. Steig[c], A. J. Schauer[c], J. Morgan[e], P. D. Neff[h], J. A. Epifanio[d], J. Severinghaus[e], M. Bender[a,i], and J. A. Higgins[a,1,2]

Affiliations are included on p. 6.

Edited by Eric W. Wolff, University of Cambridge, Cambridge, United Kingdom; received February 4, 2025; accepted August 6, 2025 by Editorial Board Member Akkihebbal R. Ravishankara

Antarctic ice cores provide a unique archive of Earth's atmosphere and its largest extant ice sheet. The oldest continuous ice core extends back 800 ky, though discontinuous ice cores from the Allan Hills blue ice area (BIA) have been shown to preserve snapshots of ice and air back to at least 2.7 million years ago (Ma). Here, we provide snapshots of putatively Miocene and Pliocene ice and air from shallow ice cores drilled in the Allan Hills BIA. The ice, dated using the deficit in ^{40}Ar in ancient air compared to the modern atmosphere, is stratigraphically complex. Nevertheless, surface temperatures inferred from water isotopes correlate with sample age and indicate 12 ± 2 °C of cooling in Antarctica between 6 Ma and the late Pleistocene. Basal ice is nearly devoid of gases and remains to be dated with existing methods. This undated ice is characterized by an isotopic temperature 5 ± 1 °C warmer than the oldest dated (6 million year old) sample. We speculate that this ice reflects surface snowpack or permafrost that was preserved by the growth of the East Antarctic ice sheet in the Middle to Late Miocene.

paleoclimate | carbon cycle | Earth history | cryosphere

Significance

Antarctic ice cores provide the most direct archive of Earth's atmosphere and its largest ice sheets. We report the discovery of ice, dated by its deficit in ^{40}Ar compared to the modern atmosphere, that is up to 6 million years old. Isotopic temperatures from this ice indicate progressive cooling over the Pliocene; enigmatic basal ice from the Miocene is characterized by even warmer temperatures and may reflect a relic from the adolescent days of the Antarctic ice sheet. This archive opens up the possibility of reconstructing Earth's climate and its largest ice sheet during periods when Earth's climate was warmer and sea-level was higher.

Antarctic ice cores play a central role in our understanding of Earth's climate system (1). The ice core record is remarkably detailed, providing information about past temperature (2, 3), ocean heat content (4–6), snow accumulation (7), atmospheric circulation (8), and sea level. The ice also traps small samples of the atmosphere, preserving a highly accurate record of greenhouse gases and other important atmospheric constituents (9, 10). Direct reconstructions from ice cores are our best evidence for a strong link between atmospheric carbon dioxide (CO_2) and Earth's climate on geologic timescales.

The oldest continuous ice cores are from East Antarctica and extend back to 800 thousand years ago (ka). There are compelling reasons to extend the ice core record to earlier times. Over the past ~15 My, Earth's climate has cooled (11). This cooling has been accompanied by the growth of the Antarctic ice sheet (12–14). However, the dynamics of this process and its relationship to important climatic variables such as atmospheric greenhouse gases or ocean heat content remain uncertain. For example, reconstructions from marine sediment cores indicate a highly dynamic Antarctic ice sheet in the Miocene (15); warm intervals of this Epoch are associated with substantial inland retreat of the ice sheet margin and the growth of tundra vegetation in ice free areas (16, 17) whereas cold intervals appear to be associated with expansion of the ice sheet and a grounding line that extended well into the Ross Sea basins (15). In particular, widespread evidence of subglacial meltwater features crossing high-altitude saddles and scoured bedrock near the coast have been interpreted to reflect a thickened and expanded Antarctic ice sheet that overrode the Transantarctic Mountains in the Miocene (13, 18–20). The history of the East Antarctic ice sheet in the Pliocene is more controversial; old cosmogenic exposure ages from sites across the Transantarctic mountains (21, 22) indicate a stable polar desert since the Miocene whereas evidence from marine sediment cores (23, 24) and numerical modeling (25–27) suggest a more dynamic East Antarctic ice sheet in the Pliocene, with periods of widespread retreat in marine based sectors.

Antarctic blue ice areas (BIAs) are promising sites for extending ice core records far beyond 800 ka. BIAs are surface outcrops of glacier ice at the margins of the Antarctic ice sheet that cover approximately 1% of the total continental area (28). The Allan Hills Main Ice Field (76.7° S, 159.3° E and 1,900 to 2,000 m above sea level) is located at the boundary between the Convoy Range of the Transantarctic Mountains and the greater East Antarctic ice sheet (Fig. 1). Although the mechanism by which old ice is preserved in BIAs is not well understood, shallow ice cores (100 to 200 m) drilled in the Allan Hills BIA in

Author contributions: E.B., M.B., and J.A.H. designed research; S.S., V.H., L.D., J.M.P., A.C., S.A., A.K., D.I., Y.Y., I.M.N., A.J.S., J.M., P.D.N., J.A.E., J.S., and J.A.H. performed research; S.S., E.B., E.J.S., J.S., and J.A.H. contributed new reagents/analytic tools; S.S., V.H., L.D., J.M.P., E.B., A.C., S.A., A.K., D.I., Y.Y., C.B., E.J.S., A.J.S., J.M., P.D.N., J.A.E., J.S., M.B., and J.A.H. analyzed data; and S.S., V.H., L.D., E.B., J.M.P., A.C., S.A., A.K., Y.Y., C.B., E.J.S., J.S., M.B., and J.A.H. wrote the paper.

The authors declare no competing interest.

This article is a PNAS Direct Submission. E.W.W. is a guest editor invited by the Editorial Board.

[1]S.S. and J.A.H. contributed equally to this work.

[2]To whom correspondence may be addressed. Email: sarah.shackleton@whoi.edu or jahiggin@princeton.edu.

This article contains supporting information online at https://www.pnas.org/lookup/suppl/doi:10.1073/pnas.2502681122/-/DCSupplemental.

Published October 28, 2025.

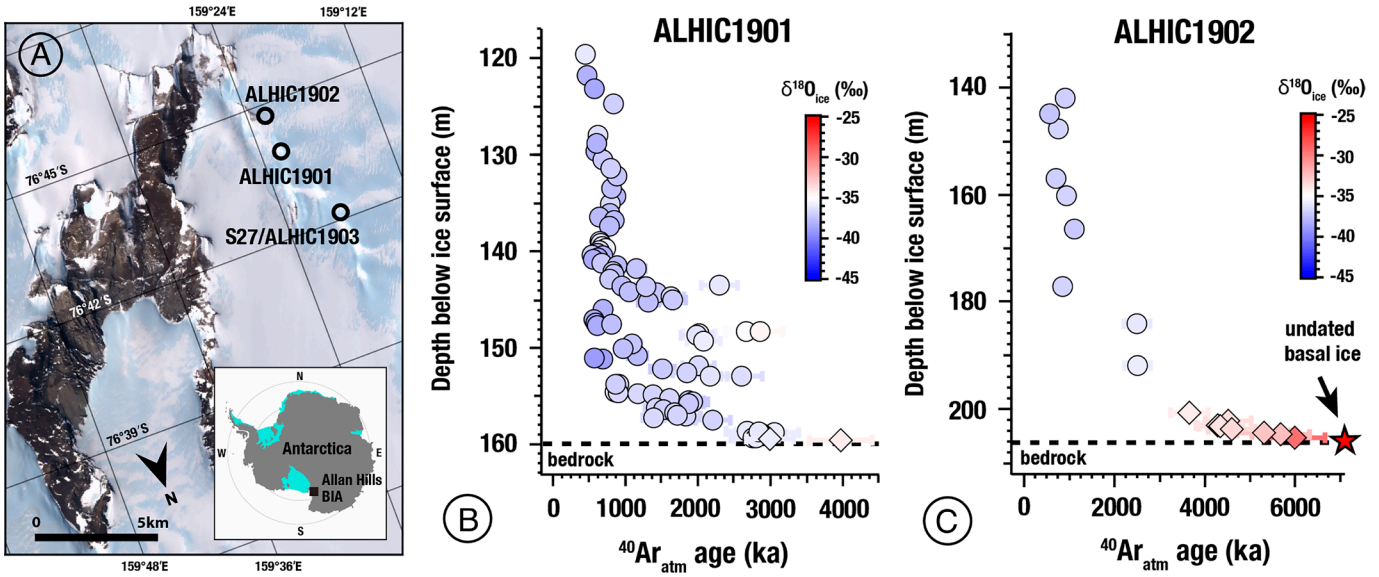

Fig. 1. (*A*) Map of the Allan Hills blue ice area (BIA) and the shallow ice cores used in this study (ALHIC1901, ALHIC1902, and ALHIC1903). (*B*) $^{40}Ar_{ATM}$ vs depth for ALHIC1901, colored by the $\delta^{18}O_{ice}$ of the sample. Uncertainties reflect absolute ages ± 1σ. Diamonds indicate samples with suspected postdepositional Ar loss. (*C*) $^{40}Ar_{ATM}$ vs depth for ALHIC1902, colored by the $\delta^{18}O_{ice}$ of the sample (scale the same as in *B*). Uncertainties reflect absolute ages ± 1σ (~11% of sample age). Diamonds indicate samples with suspected postdepositional Ar loss.

areas associated with slow surface ice flow and steep bedrock topography preserve ice and air that is at least 2.7 million years old (29, 30).

Here, we report the chronologies ($^{40}Ar_{atm}$) and isotopic composition of ice ($\delta^{18}O_{ice}$, δD_{ice}) from three new ice cores drilled in the Allan Hills BIA during the 2019–2020 and 2022–2023 field seasons (Fig. 1*A*). Allan Hills Ice Core (ALHIC) 1901 (76.732376° S, 159.356125 °E) was drilled to bedrock at 159 m depth using the U.S. Ice Drilling Program (IDP) 24 cm blue ice drill (31) adjacent to Site BIT58/ALHIC1503, where (29, 30) recovered basal ice with $^{40}Ar_{atm}$ ages as far back as 2.7 million years ago (Ma). ALHIC1902 (76.745357° S, 159.374108 °E) was drilled to bedrock at 206 m depth using the U.S. IDP 10 cm FORO (32) drill at a site adjacent to a nunatak. ALHIC1903 (76.702435° S, 159.310603° E) was drilled to a depth of 150 m using the U.S. IDP 24 cm blue ice drill adjacent to Site S27 (29, 30, 33), a site that preserves a continuous ice core record between 115 and 250 ka. ALHIC1903 provides a critical frame of reference for ice core paleoclimate studies in the Allan Hills BIA as the trapped gases preserve the full range of glacial-interglacial variability from the penultimate ice age and its termination.

We date the ice and trapped gases directly, taking advantage of the secular increase in the ^{40}Ar content of the atmosphere over Earth history due to the decay of ^{40}K in Earth's interior [the $^{40}Ar_{atm}$ geochronometer; (34)]. Processes that result in mass-dependent fractionation of argon—namely, the gravitational settling of gases in the firn—are corrected for by analyzing the two stable isotopes of argon (^{36}Ar and ^{38}Ar) in addition to radiogenic ^{40}Ar (*SI Appendix*, sections 1.1 and 2). This chronometer is calibrated only over 0-800 ka; uncertainties in this calibration represent the largest source of error in the absolute ages of samples older than ~600 ka (~11% of sample age 1σ; Dataset S1). Relative age uncertainties are an order of magnitude smaller (~60 ky; 1σ). We disregard the difference in age between the ice and the gas trapped within it because it is smaller, by an order of magnitude or more, than the dating uncertainty.

The isotopic composition of Antarctic precipitation ($\delta^{18}O_{ice}$ and δD_{ice}) provides information about both local temperature and the temperature where precipitation originates (35, 36). The use of water isotopes as a temperature proxy derives from the fundamental role temperature plays in the physical processes involved in the hydrological cycle (37) and the strong empirical correlation between $\delta^{18}O_{ice}$ and Antarctic surface temperatures (2, 35). Deuterium excess (d_{xs}), the weighted difference between $\delta^{18}O_{ice}$ and δD_{ice} ($d_{xs} = \delta^{18}O_{ice} - 8*\delta D_{ice}$), reflects the temperature of the source of moisture evaporation (38). Together, $\delta^{18}O_{ice}$ and δD_{ice} can be used to explore latitudinal temperature gradients (polar amplification), changes in mean latitude of moisture sources, and ice sheet elevation [(35, 36); *SI Appendix*, section 4]. $\delta^{18}O_{ice}$ and d_{xs} values from the Allan Hills BIA may also be susceptible to postdepositional alteration by sublimation at the accumulation site (39). However, sublimation is not required to explain the negative d_{xs} values observed at the Allan Hills BIA and, if present, does not appear to result in any bias in associated gas records (29, 30).

Pliocene and Miocene ice from the Allan Hills BIA

As shown in Fig. 1 and *SI Appendix*, Fig. S1, and listed in Dataset S1, ALHIC1901, ALHIC1902, and ALHIC1903 preserve ice with $^{40}Ar_{atm}$ ages that range from the Late Pleistocene (ALHIC1903) to the Early Pliocene (ALHIC1901) to the Late Miocene (ALHIC1902). Measured $^{40}Ar_{atm}$ ages for ALHIC1903 (110 ± 70 ka 1σ; N = 13) agree well with independent chronologies of this core from atmospheric trace gases [CO_2, $\delta^{18}O_{atm}$, and CH_4 (40)] and water isotopes (33). ALHIC1901 and ALHIC1902 both contain ice that is much older and stratigraphically discontinuous. At both sites we focused on ice near the bedrock in line with previous studies (29, 30). $^{40}Ar_{atm}$ ages increase from 400 to 800 ka at 120 to 140 m to 4.0 ± 0.4 Ma at bedrock in ALHIC1901 (159 m) and 6.0 ± 0.7 Ma at ~90 cm above bedrock in ALHIC1902 (206 m). In ALHIC1901 the age–depth relationship is complex, with multiple instances of inverted stratigraphy (older ice on top of younger ice). In contrast, in ALHIC1902, the age–depth relationship is characterized by a progressive increase in $^{40}Ar_{atm}$ age with depth, although this may be an artifact of the lower-resolution chronology compared to ALHIC1901.

All samples older than ~2.7 Ma from both sites show some evidence for postdepositional Ar loss as indicated by elevated Kr/Ar

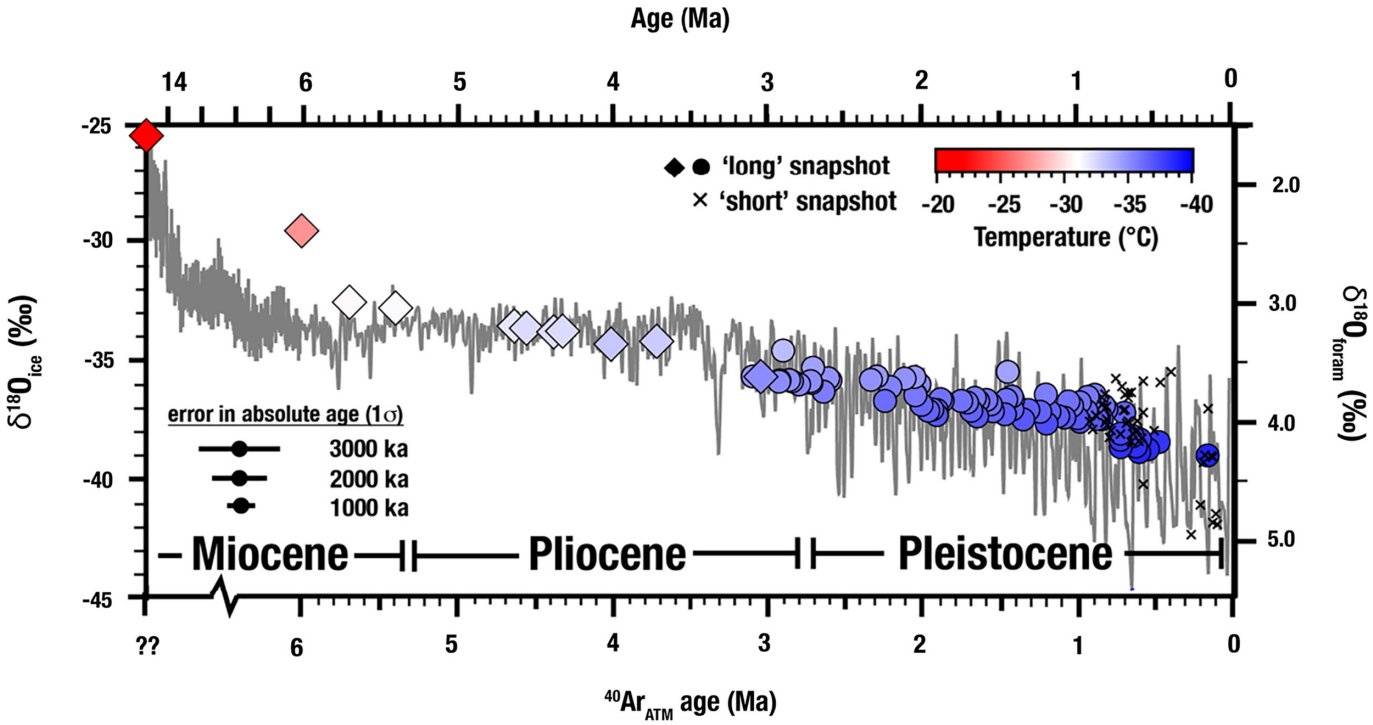

Fig. 2. Time series of $^{40}Ar_{ATM}$ ages and $\delta^{18}O_{ice}$ values for Allan Hills ice cores ALHIC1901, ALHIC1902, ALHIC1903, and ALHIC1503 (29) time-integrated snapshots of the mean climate state shown in filled circles (●) and diamonds (◆) whereas "short" snapshots of paleoclimate properties shown as (x; see text for details). Color indicates estimate of mean annual temperature using the water isotope-temperature calibration from (35). Absolute temperature uncertainties are ±5 °C whereas relative uncertainties are much smaller (<2 to 3 °C; Dataset S1). Uncertainties in absolute ages ±11% (1σ) for samples >600 ka. Relative age uncertainties are much smaller (~60 ky; 1σ). Also plotted is the stacked record of benthic foraminiferal $\delta^{18}O_{CaCO3}$ values from (44). Diamonds indicate samples with suspected postdepositional Ar loss.

ratios and depleted Ar/N_2 ratios (Dataset S1). The extent of Ar loss correlates with $^{38}Ar/^{36}Ar$ ratios, Xe loss, sample age (older samples have experienced greater Ar and Xe loss). These effects are qualitatively similar but differ in detail from site-to-site, suggesting that the alteration occurred locally. The cause of this Ar loss remains unknown, though our preferred explanation is that it reflects the removal of melt (and dissolved Ar and Xe) along grain boundaries during periods when the local ice sheet was significantly thicker than present (*SI Appendix*, section 3). Regardless of its origins, the Ar loss is unlikely to result in a significant bias in measured $^{40}Ar_{atm}$ ages as the process appears to be mass-dependent and can be corrected using simultaneous measurements of ^{38}Ar and ^{36}Ar akin to the correction for gravitational fractionation of Ar isotopes in the firn.

The bottom ~1.5 m of ALHIC1902 is unique relative to all other previously recovered basal ice at the Allan Hills BIA; it is associated with a visible increase in sediment/dust content and an abrupt decline in total air content from ~0.08 to 0.09 cc air/g ice at 205 m (5.3 to 5.7 Ma) to 0.02 cc air/g ice at 205.45 m (6.0 Ma) and <0.001 cc air/g at 206.4 m (undated). Although the small amount of gas in the deepest ice sample prevented determination of a $^{40}Ar_{atm}$ age, elemental (Ar/N_2 and O_2/N_2) and isotopic ratios ($\delta^{15}N$ of N_2) were analyzed to assist in identifying the processes responsible for gas loss. Measured Ar/N_2, O_2/N_2, and $\delta^{15}N$ of N_2 for this sample are +961‰, −463‰, and +1.3‰ relative to the modern atmosphere. All these values are too large in amplitude to be explained by atmospheric or firn processes, and therefore must represent alteration near the bed. The Ar/N_2 ratio and elevated $\delta^{15}N$ of N_2 reflect saturation of refrozen meltwater (41) and the low O_2/N_2 reflects metabolic O_2 consumption (42).

Measured $\delta^{18}O_{ice}$ values from all Allan Hills ice cores [ALHIC1901/1902/1903 and ALHIC1503 (29)] are plotted against $^{40}Ar_{atm}$ ages of the same samples in Fig. 2. $\delta^{18}O_{ice}$ values range from −42.5‰ during the penultimate glacial maximum (0.14 Ma) to −37.0‰ during the last interglacial (0.13 Ma) in ALHIC1903, with a depth-weighted average across the penultimate glacial termination of −38.7‰. $\delta^{18}O_{ice}$ values for Pleistocene ice (<2.7 Ma) from both ALHIC1901 and ALHIC1902 range from −38.9 to −35.3‰. $\delta^{18}O_{ice}$ values for Pliocene ice (2.7 to 5.2 Ma) range from −36.0 to −33.5‰ and $\delta^{18}O_{ice}$ values for Miocene ice (>5.2 Ma) range from −32.8 to −25.2‰. The highest $\delta^{18}O_{ice}$ value comes from the deepest (undated) ice sample. All samples fall on a local meteoric water line (MWL; $\delta^{18}O_{ice}$ vs δD_{ice}) with a slope of 8.92 ± 0.11 (95%), slightly higher than, the MWL associated with ice cores from the Antarctic interior (7.75 to 8.23 (35, 43); *SI Appendix*, section 5).

Converting ice core $\delta^{18}O_{ice}$ to surface temperature (T_S) relies on the temporal regression slope between these two parameters, which under favorable conditions can be derived from borehole thermometry (45) or thermal fractionation in $\delta^{15}N$ of N_2 (46). In the Allan Hills, these constraints are unavailable, so we instead consider the modern spatial $\delta^{18}O_{ice}$–T_S regression slope and an independent constraint on the temporal glacial-interglacial slope from the Talos Dome ice core (47), the deep ice core record nearest to the Allan Hills. An empirical database of the isotopic composition of modern Antarctic surface snow and mean annual surface temperature provides a spatial $\delta^{18}O_{ice}$–T_S regression slope of 0.80‰ °C^{-1} [MD08; (35)]. While recent work shows that the use of the spatial slope may overestimate T_S variations in interior East Antarctica (36, 48, 49) the calculated $\delta^{18}O_{ice}$–T_S temporal slope at Talos Dome is 0.88‰ °C^{-1} (49), similar to the spatial regression slope. We therefore use 0.80‰ °C^{-1} and assume a 15% uncertainty (1σ) following (50) and assume that global climatological $\delta^{18}O_{ice}$–T_S relationships are the same as present. Temperature reconstructions are corrected for changes in the $\delta^{18}O$ of seawater ($\delta^{18}O_{sw}$) estimated from benthic foraminiferal $\delta^{18}O_{CaCO3}$ records (*SI Appendix*, section 4). Different assumptions about the

history of the $\delta^{18}O_{sw}$ alter the reconstructed temperatures presented here by no more than 1 °C.

Our results provide Antarctic ice core records that extend into the Miocene. Uncertainties in $^{40}Ar_{atm}$ ages arise from the extrapolation of an empirical calibration of atmospheric ^{40}Ar over the last 800 ky, the potential for contamination from radiogenic ^{40}Ar, in the underlying continental crust (42), and the potential for slight differences in the mass dependence of Ar isotope fractionation associated with Ar loss in samples older than ~2.7 Ma. In spite of these uncertainties, we interpret $^{40}Ar_{atm}$ ages as robust evidence for ice and trapped air that dates to the Miocene and Pliocene for three reasons. First, although the ice is stratigraphically complex, the general stratigraphy indicates preservation of the oldest ice samples near the bedrock. Second, $\delta^{18}O_{ice}$ values increase with $^{40}Ar_{atm}$ age, even in ice that is stratigraphically complex (Fig. 1), consistent with the expectation of a warmer East Antarctica in the Pliocene and Miocene. Third, while there is evidence for Ar loss in the oldest samples, this process should be mass dependent and accounted for with measured $^{38}Ar/^{36}Ar$ ratios. Although the mass dependence of this Ar loss could, in principle, differ from gravitational fractionation in the firn, we recover the same relationship between $^{40}Ar_{atm}$ ages and $\delta^{18}O_{ice}$ values at both sites in spite of significant differences in the extent of Ar loss (Fig. 2).

Other potential sources of uncertainty in the $^{40}Ar_{atm}$ geochronometer such as the addition of radiogenic ^{40}Ar from the underlying crust [in situ production of ^{40}Ar from dust and sediment within the ice is negligible; (42)] will result in an underestimate of sample age. For example, basal ice from GISP2 in Greenland contains excess ^{40}Ar equivalent to a future $^{40}Ar_{atm}$ age of 4.5 to 6 My. However, the bedrock underlying GISP2 is Proterozoic granite (high K and old age) whereas the local bedrock at the Allan Hills is composed of Jurassic mafic volcaniclastic rocks [(51); low K and young age].

Paleoclimate Records From Stratigraphically Disturbed Ice

The preservation of Pliocene and Miocene ice and air in the Allan Hills BIA opens the exciting possibility of extending direct reconstructions of Earth's atmosphere and the Antarctic ice sheet into warmer periods of Earth's history. However, we are presently unable to completely decode the record. We lack information about the orientation of preserved layering, the amount of time represented in an individual sample, and the extent of mixing and diffusion between samples of different ages. In addition, interglacial accumulation rates are an order of magnitude higher across MIS5/6 in nearby site S27/ALHIC1903, suggesting that older discontinuous records may also contain a climate-dependent preservation bias.

The loss of stratigraphic continuity and extreme depth gradients in ice age (up to 100 s of ky/cm; *SI Appendix*, Fig. S2) observed in shallow ice cores from the Allan Hills BIA is presumed due to thinning and folding on various length-scales during transport from nearby source regions. The result is an increase in the amount of time preserved in each volume of ice (age density or y/cm) and the complicated age–depth relationships observed in ALHIC1901. The age density (y/cm) in Allan Hills ice cores increases by >6 orders of magnitude between stratigraphically continuous ice from ALHIC1903/S27 and the discontinuous old (>800 ka) ice from ALHIC1901 (*SI Appendix*, Fig. S2). In ALHIC1903/S27 the age density overlaps with continuous ice cores from the interior (1 to 10 y/cm) whereas the age density in ALHIC1901 is up to 5 orders of magnitude higher (1,000 to 100,000 y/cm). Age density also appears to increase with depth in both continuous and discontinuous ice cores. In ALHIC1903/S27 the increase is gradual and can primarily be attributed to thinning whereas in ALHIC1901 age-density increases abruptly by an order of magnitude at ~140 m depth. This increase likely involves both thinning and folding (*SI Appendix*, Fig. S2, *Inset*), as well as lower accumulation of glacial ice. In the deepest ice, the estimated age density approaches 100 ky/cm, indicating that discrete, cm-scale samples of this ice may represent averages over glacial cycles ("long" snapshots). In shallower and younger ice, age densities of 1 to 10 ky/cm may preserve more (though likely not all) of the true glacial-interglacial variability ("short" snapshots).

This interpretative framework for climate archives in discontinuous shallow ice cores from the Allan Hills BIA is tentative and requires further evaluation with measurements of trapped gases and other ice core properties. However, three lines of evidence from $\delta^{18}O_{ice}$ measurements support our hypothesis of high age densities (>1 ky/cm), the existence of both "short" and "long" snapshots, and a slight interglacial preservation bias (Dataset S1). First, ice younger than 800 ka but stratigraphically below the increase in age density at ~140 m in ALHIC1901 records much less variability in $\delta^{18}O_{ice}$. Second, glacial values of $\delta^{18}O_{ice}$ are absent in both "short" and "long" snapshots in ice younger than 800 ka. Third, average values of $\delta^{18}O_{ice}$ for "long" snapshots (–38.5‰) show good agreement with the accumulation rate-weighted average from S27/ALHIC1903 across MIS5/6 (–38.7‰). In the absence of evidence to the contrary, we assume that the interglacial bias has remained constant over the interval represented in our cores.

A >6-My Record of Surface Temperatures in East Antarctica

Temperatures derived from $\delta^{18}O_{ice}$ values measured in the Allan Hills ice cores provide direct reconstruction of East Antarctic climate during the Miocene and Pliocene Epochs. While temperatures from $\delta^{18}O_{ice}$ values are also sensitive to changes in the elevation of the ice sheet due to local uplift or subsidence, evidence from the sites around the Transantarctic Mountains (52) including the present-day elevation of subaerially erupted lava flows (20, 53) indicate that uplift has been less than a few hundred meters since the Middle to Late Miocene. As a result, we interpret our record as primarily preserving an interglacially biased temperature history of East Antarctica near the Transantarctic Mountains from the Late Miocene to the Late Pleistocene.

Reconstructed temperatures from ice cores in the Allan Hills BIA indicate that there has been ~12 ± 2 °C of cooling in East Antarctica over the last 6 million years (Fig. 3). This cooling is roughly equally partitioned between the Late Miocene (4 ± 1 °C between 6.0 and

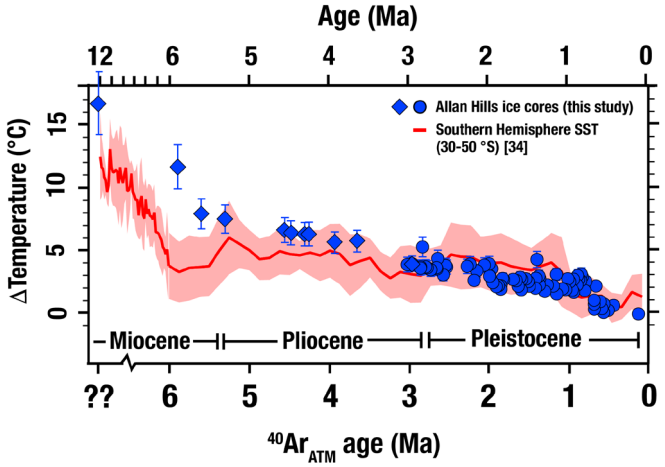

Fig. 3. Time series of East Antarctic temperatures from Allan Hills ice cores (●) and Southern Ocean sea-surface temperatures (–) from (54). Note the apparent polar amplification of cooling in East Antarctica during the Late Miocene and Pliocene (though this may partly reflect changes in ice surface elevation). Diamonds indicate samples with suspected postdepositional Ar loss.

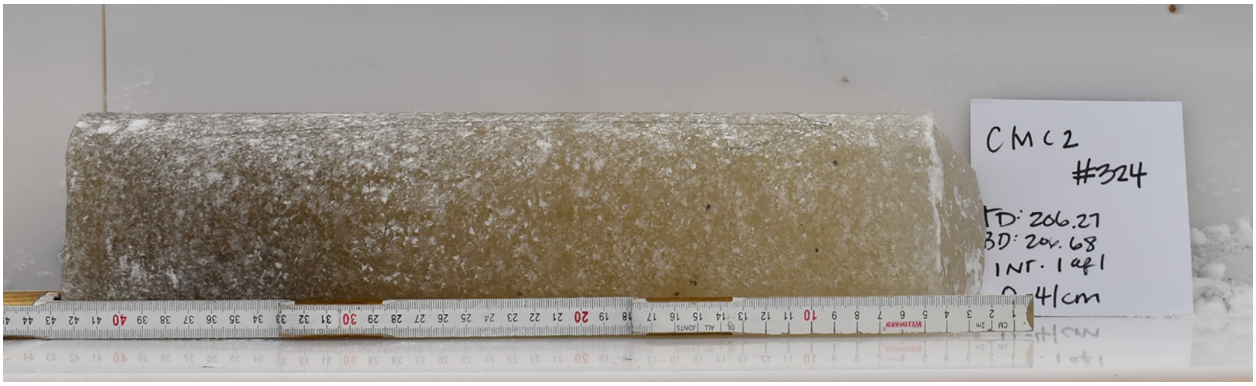

Fig. 4. Dirty basal ice from 206 m in ALHIC1902. The ice sits stratigraphically below ice with a 6-Ma $^{40}Ar_{ATM}$ age. We speculate that this basal ice represents local snowpack or permafrost from the Middle to Late Miocene that was entombed by the growth of the East Antarctic ice sheet. The index card references the field ID (CMC2) rather than the core ID (ALHIC1902).

5.3 Ma), the Pliocene (4 ± 1 °C of cooling between 5.3 to 2.7 Ma), and the Pleistocene (4 ± 1 °C of cooling over the last 2.7 million years). The magnitude of cooling is similar to, though somewhat larger than, the cooling observed in Southern Hemisphere sea surface temperatures over the same time period (54). The apparent amplification of cooling in East Antarctica is most obvious in the Late Miocene, though it may extend throughout the Pliocene. Determining both the magnitude and timing of changes in polar amplification is beyond the scope of this study though we note that these records may provide a unique opportunity to directly test hypotheses on the extent and dynamism of the East Antarctic ice sheet during the Late Miocene and Pliocene (23, 27).

Ice Core Evidence for Mid-Late Miocene Growth of the East Antarctic Ice Sheet

The undated basal ice is particularly enigmatic, though it shares some similar characteristics to the dirty basal ice recovered from ice cores in Greenland (42, 55). First, it has experienced significant (>98%) gas loss and contains more silt compared to shallower ice (Fig. 4). Gas loss appears to have occurred through melting and bubble migration as indicated by the elevated $\delta^{15}N$ of N_2 and Ar/N_2 of the residual air. Second, the $\delta^{18}O_{ice}$ value (–25‰) is the highest in any sample yet analyzed from Allan Hills ice cores, with estimates of mean annual temperature that are 5 ±1 °C warmer than the overlying 6 Ma ice and 18 ± 3 °C warmer than the average of the Late Pleistocene, respectively. Third, the ice lies on the local meteoric water line for the Allan Hills BIA (Dataset S1), suggesting that any postdepositional alteration by melting and/or refreezing is minor (55).

Given these characteristics the most plausible explanation for origin of the gas-less basal ice in ALHIC1902 is that it represents local snowpack or permafrost from the Middle to Late Miocene that was entombed by the growth of the East Antarctic ice sheet in the Middle to Late Miocene (13, 19, 20, 56). Alternative explanations such as melting and gas loss under a locally thickened East Antarctic ice sheet are less likely; this overriding ice sheet would have to be at least 2,000 m thicker in the Allan Hills BIA, raising the ground surface to >3,200 m after isostatic adjustment. Even allowing for some tectonic uplift, a large ice sheet at this elevation is difficult to reconcile with the warm surface temperatures implied by a $\delta^{18}O_{ice}$ value of –25‰.

Conclusions

The discovery of 6 million year old ice and air in shallow ice cores drilled in the Allan Hills BIA on the margin of the East Antarctic ice sheet shows that it is possible to extend direct reconstructions of Earth's atmosphere and its largest ice sheet into periods where Earth's climate was warmer and global sea-level was higher. However, discontinuous ice cores from marginal BIAs are stratigraphically complex and our understanding of the potential for bias and completeness of the archive is in its early days. Isotopic temperatures from this ice indicate cooling over the Pliocene that is similar in magnitude to records from marine sediments in the Southern Ocean. Enigmatic gas-less basal ice is characterized by an isotopic temperature that is >15 °C warmer than the late Pleistocene average and likely represents Mid to Late Miocene surface snowpack or permafrost that was preserved by the subsequent growth of the East Antarctic ice sheet. Future research on these ice cores have the potential to provide unique insight into many fundamental questions in paleoclimate science including the history and stability of the Antarctic ice sheet and its relationship to atmospheric greenhouse gases and mean ocean temperature with direct implications for future projections of sea-level rise, ocean circulation, and global radiative forcing.

Methods

Gas Analysis. Ice core samples from ALHIC1901 (500 to 600 g) and ALHIC1902 (200 to 600g) were analyzed at Princeton University for atmospheric ^{40}Ar using established protocols ((29, 34), *SI Appendix*, section 1.1). Samples were trimmed and melted under vacuum, with released gases cryogenically trapped, purified, and measured on a Thermo Scientific 253plus dual inlet mass spectrometer. Large (>500 g) samples were processed following standard methods, with corrections for pressure imbalance and ^{40}Ar tailing applied, as described previously (*SI Appendix*, section 1.1). Smaller (200 to 300 g) ALHIC1902 samples were prepared similarly but with modifications to improve transfer efficiency into the mass spectrometer: gases were trapped on small silica gel-filled glass volumes and analyzed at lower (approximately half) running pressure, which precluded precise Xe/Kr measurements (*SI Appendix*, section 1.2). Major gas elemental and isotopic ratios from the deepest undated ALHIC1902 sample were measured at Scripps Institution of Oceanography on a Delta XP dual inlet mass spectrometer with methods adapted for small volume samples (*SI Appendix*, section 1.4).

Water Isotope Analysis. Following gas extraction, meltwater from all samples measured at Princeton University was collected and analyzed for stable water isotopes ($\delta^{18}O_{ice}$, δD_{ice}) by laser spectroscopy. Measurements were performed at the Climate Change Institute at the University of Maine using established procedures (*SI Appendix*, section 1.3).

Data, Materials, and Software Availability. All study data are included in the article and/or supporting information.

ACKNOWLEDGMENTS. This work was supported by the U.S. National Science Foundation (NSF) awards 1744993, 1745007, 1744832 and the NSF Center for Oldex Ice Exploration (NSF COLDEX), an NSF Science and Technology Center (NSF-2019719). Drilling support was provided by the NSF Ice Drilling Program (NSF

cooperative agreements 1836328 & 2318480). We are indebted to Elizabeth Morton, Tanner Kuhl, Mike Jayred, and Andrew Haala for their hard work and positive energy in the field. We thank the NSF Office of Polar Programs, the NSF Office of Integrative Activities, and Oregon State University for financial and infrastructure support. We thank the U.S. Antarctic Program for providing logistical support. We are grateful to Anna Zajicek, Jonathan Hayden, Ema Mayo, and Ash Goverman for keeping us safe, warm, and happy in the field. Special thanks go to Troy Juniel, Dave Ferris, and their teams for ensuring our ice cores remained safe, cold, and well cared for both in McMurdo and during transport to our freezers. Ice core storage and curation were provided by the NSF Ice Core Facility (NSF-2041950). We especially thank Richard Nunn, Curt LaBombard, and Theo Carr for their assistance processing these complex records. We also thank Sergey Oleynik for laboratory assistance. Finally, we acknowledge COLDEX team members for their valuable support, guidance, and feedback throughout the preparation and publication of this work.

Author affiliations: [a]Department of Geosciences, Princeton University, Princeton, NJ 08544; [b]Department of Geology & Geophysics, Woods Hole Oceanographic Institution, Woods Hole, MA 02543; [c]Department of Earth & Space Sciences, University of Washington, Seattle, WA 98195; [d]College of Earth, Ocean, and Atmospheric Sciences, Oregon State University, Corvallis, OR 97331; [e]Scripps Institution of Oceanography, University of California San Diego, La Jolla, CA 92093; [f]Climate Change Institute, University of Maine, Orono, ME 04469; [g]State Key Laboratory of Marine Geology, Tongji University, Shanghai 200092, China; [h]Department of Soil, Water, and Climate, University of Minnesota, St. Paul, MN 55108; and [i]School of Oceanography, Shanghai Jiao Tong University, Shanghai 200240, China

1. E. J. Brook, C. Buizert, Antarctic and global climate history viewed from ice cores. *Nature* **558**, 200–208 (2018).
2. J. Jouzel *et al.*, Vostok ice core–A continuous isotope temperature record over the last climatic cycle (160, 000 years). *Nature* **329**, 403–408 (1987).
3. J. Jouzel *et al.*, Orbital and millennial Antarctic climate variability over the past 800, 000 years. *Science* **317**, 793–796 (2007).
4. M. A. Headly, J. P. Severinghaus, A method to measure Kr/N2 ratios in air bubbles trapped in ice cores and its application in reconstructing past mean ocean temperature. *J. Geophys. Res.–Atmos.* **112**, D19105 (2007), 10.1029/2006JD008317.
5. B. Bereiter, S. Shackleton, D. Baggenstos, K. Kawamura, J. Severinghaus, Mean global ocean temperatures during the last glacial transition. *Nature* **553**, 39–44 (2018).
6. S. Shackleton *et al.*, Global ocean heat content in the last interglacial. *Nat. Geosci.* **13**, 77–81 (2020).
7. T. D. Van Ommen, V. Morgan, M. A. Curran, Deglacial and holocene changes in accumulation at Law Dome. *Ann. Glaciol.* **39**, 359–365 (2004).
8. J.-R. Petit, M. Briat, A. Royer, Ice age aerosol content from East Antarctic ice core samples and past wind strength. *Nature* **293**, 391–394 (1981).
9. J. R. Petit *et al.*, Climate and atmospheric history of the past 420, 000 years from the Vostok ice core, *Antarctica*. *Nature* **399**, 429–436 (1999).
10. EPICA, Eight glacial cycles from an Antarctic Ice Core. *Nature* **429**, 623–628 (2004).
11. J. Zachos, M. Pagani, L. Sloan, E. Thomas, K. Billups, Trends, rhythms, and aberrations in global climate 65 Ma to present. *Science* **292**, 686–693 (2001).
12. K. G. Miller *et al.*, Cenozoic sea-level and cryospheric evolution from deep-sea geochemical and continental margin records. *Sci. Adv.* **6**, eaaz1346 (2020).
13. G. H. Denton, M. L. Prentice, D. E. Kellogg, T. B. Kellogg, Late tertiary history of the Antarctic ice sheet: Evidence from the Dry Valleys. *Geology* **12**, 263–267 (1984).
14. C. H. Lear *et al.*, Neogene ice volume and ocean temperatures: Insights from infaunal foraminiferal Mg/Ca paleothermometry. *Paleoceanography* **30**, 1437–1454 (2015).
15. S. Passchier *et al.*, Early and middle Miocene Antarctic glacial history from the sedimentary facies distribution in the AND-2A drill hole, Ross Sea. *Geol. Soc. Am. Bull.* **123**, 2352–2365 (2011).
16. R. Levy *et al.*, Antarctic ice sheet sensitivity to atmospheric CO2 variations in the early to mid-Miocene. *Proc. Nat. Acad. Sci.* **113**, 3453–3458 (2016).
17. S. J. Feakins, S. Warny, J.-E. Lee, Hydrologic cycling over Antarctica during the middle Miocene warming. *Nat. Geosci.* **5**, 557–560 (2012).
18. G. H. Denton, D. E. Sugden, D. R. Marchant, B. L. Hall, T. I. Wilch, East Antarctic Ice Sheet sensitivity to Pliocene climatic change from a Dry Valleys perspective. *Geogr. Ann. Ser. A Phys. Geogr.* **75**, 155–204 (1993).
19. D. Sugden, G. Denton, Cenozoic landscape evolution of the Convoy Range to Mackay Glacier area, Transantarctic Mountains: Onshore to offshore synthesis. *GSA Bull.* **116**, 840–857 (2004).
20. G. H. Denton, D. E. Sugden, Meltwater features that suggest miocene ice-sheet overriding of the transantarctic mountains in victoria land, antarctica. *Geografiska Annaler: Ser. A, Phys. Geogr.* **87**, 67–85 (2005).
21. A. Balter-Kennedy, G. Bromley, G. Balco, H. Thomas, M. S. Jackson, A 14.5-million-year record of East Antarctic Ice Sheet fluctuations from the central Transantarctic Mountains, constrained with cosmogenic 3 He, 10 Be, 21 Ne, and 26 Al. *Cryosphere* **14**, 2647–2672 (2020).
22. G. Bromley, G. Balco, M. Jackson, A. Balter-Kennedy, H. Thomas, East antarctic ice sheet variability in the central transantarctic mountains since the mid miocene. *Clim. Past Discuss.* **2024**, 1–26 (2024).
23. C. P. Cook *et al.*, Dynamic behaviour of the East Antarctic ice sheet during Pliocene warmth. *Nat. Geosci.* **6**, 765–769 (2013).
24. M. O. Patterson *et al.*, Orbital forcing of the East Antarctic ice sheet during the pliocene and early pleistocene. *Nat. Geosci.* **7**, 841–847 (2014).
25. A. M. Dolan, B. De Boer, J. Bernales, D. J. Hill, A. M. Haywood, High climate model dependency of Pliocene Antarctic ice-sheet predictions. *Nat. Commun.* **9**, 2799 (2018).
26. B. de Boer *et al.*, Simulating the Antarctic ice sheet in the late-Pliocene warm period: PLISMIP-ANT, an ice-sheet model intercomparison project. *Cryosphere Discuss.* **8**, 5539–5588 (2014).
27. N. R. Golledge *et al.*, Antarctic climate and ice-sheet configuration during the early Pliocene interglacial at 4.23 Ma. *Clim. Past* **13**, 959–975 (2017).
28. R. Bintanja, On the glaciological, meteorological, and climatological significance of Antarctic blue ice areas. *Rev. Geophys.* **37**, 337–359 (1999).
29. Y. Yan *et al.*, Two-million-year-old snapshots of atmospheric gases from Antarctic ice. *Nature* **574**, 663–666 (2019).
30. J. A. Higgins *et al.*, Atmospheric composition 1 million years ago from blue ice in the Allan Hills, Antarctica. *Proc. Natl. Acad. Sci. U.S.A.* **112**, 6887–6891 (2015).
31. T. W. Kuhl *et al.*, A new large-diameter ice-core drill: The Blue Ice Drill. *Ann. Glaciol.* **55**, 1–6 (2014).
32. J. A. Johnson, A. J. Shturmakov, T. W. Kuhl, N. B. Mortensen, C. J. Gibson, Next generation of an intermediate depth drill. *Ann. Glaciol.* **55**, 27–33 (2014).
33. N. E. Spaulding *et al.*, Climate archives from 90 to 250 ka in horizontal and vertical ice cores from the Allan Hills Blue Ice Area, Antarctica. *Quatern. Res.* **80**, 562–574 (2013).
34. M. L. Bender, B. Barnett, G. Dreyfus, J. Jouzel, D. Porcelli, The contemporary degassing rate of Ar-40 from the solid Earth. *Proc. Natl. Acad. Sci. U.S.A.* **105**, 8232–8237 (2008).
35. V. Masson-Delmotte *et al.*, A review of Antarctic surface snow isotopic composition: Observations, atmospheric circulation, and isotopic modeling. *J. Climate* **21**, 3359–3387 (2008).
36. B. R. Markle, E. J. Steig, Improving temperature reconstructions from ice-core water-isotope records. *Clim. Past* **18**, 1321–1368 (2022).
37. W. Dansgaard, Stable isotopes in precipitation. *Tellus* **16**, 436–468 (1964).
38. F. Vimeux *et al.*, A 420, 000 year deuterium excess record from EAst Antarctica: Information on past changes in the origin of precipitation at Vostok. *J. Geophys. Res.–Atmos.* **106**, 31,863–31,873 (2001).
39. J. Hu, Y. Yan, L. Y. Yeung, S. G. Dee, Sublimation origin of negative deuterium excess observed in snow and ice samples from McMurdo Dry Valleys and Allan Hills Blue Ice Areas, East Antarctica. *J. Geophys. Res. Atmos.* **127**, e2021JD035950 (2022).
40. Y. Yan *et al.*, Enhanced moisture delivery into Victoria Land, East Antarctica during the early last interglacial: Implications for West Antarctic ice sheet stability. *Clim. Past Discuss.* **17**, 1–23 (2021).
41. C. E. Klots, B. B. Benson, Isotope effect in the solution of oxygen and nitrogen in distilled water. *J. Chem. Phys.* **38**, 890–892 (1963).
42. M. L. Bender, E. Burgess, R. B. Alley, B. Barnett, G. D. Clow, On the nature of the dirty ice at the bottom of the GISP2 ice core. *Earth Planet. Sci. Lett.* **299**, 466–473 (2010).
43. B. Stenni *et al.*, The deuterium excess records of EPICA Dome C and Dronning Maud Land ice cores (East Antarctica). *Quatern. Sci. Rev.* **29**, 146–159 (2010).
44. T. Westerhold *et al.*, An astronomically dated record of Earth's climate and its predictability over the last 66 million years. *Science* **369**, 1383–1387 (2020).
45. K. M. Cuffey *et al.*, Deglacial temperature history of West Antarctica. *Proc. Natl. Acad. Sci.* **113**, 14249–14254 (2016).
46. J. P. Severinghaus, T. Sowers, E. J. Brook, R. B. Alley, M. L. Bender, Timing of abrupt climate change at the end of the Younger Dryas interval from thermally fractionated gases in polar ice. *Nature* **391**, 141–146 (1998).
47. B. Stenni *et al.*, Expression of the bipolar see-saw in Antarctic climate records during the last deglaciation. *Nat. Geosci.* **4**, 46–49 (2011).
48. E. C. Kahle *et al.*, Reconstruction of temperature, accumulation rate, and layer thinning from an ice core at South Pole, using a statistical inverse method. *J. Geophys. Res. Atmos.* **126**, e2020JD033300 (2021).
49. C. Buizert *et al.*, Antarctic surface temperature and elevation during the Last Glacial Maximum. *Science* **372**, 1097–1101 (2021).
50. J. Jouzel *et al.*, Magnitude of isotope/temperature scaling for interpretation of central Antarctic ice cores. *J. Geophys. Res. Atmos.* **108**, 2002JD002677 (2003).
51. P.-S. Ross, J. D. L. White, M. McClintock, Geological evolution of the Coombs-Allan Hills area, Ferrar large igneous province, Antarctica: Debris avalanches, mafic pyroclastic density currents, phreatocauldrons. *J. Volcanol. Geotherm. Res.* **172**, 38–60 (2008).
52. E. J. Brook *et al.*, Constraints on age, erosion, and uplift of Neogene glacial deposits in the Transantarctic Mountains determined from in situ cosmogenic 10Be and 26Al. *Geology* **23**, 1063–1066 (1995).
53. T. I. Wilch, D. R. Lux, G. H. Denton, W. C. McIntosh, Minimal pliocene-pleistocene uplift of the dry valleys sector of the Transantarctic Mountains: A key parameter in ice-sheet reconstructions. *Geology* **21**, 841–844 (1993).
54. T. D. Herbert *et al.*, Late Miocene global cooling and the rise of modern ecosystems. *Nat. Geosci.* **9**, 843–847 (2016).
55. R. Souchez *et al.*, Stable isotopes in the basal silty ice preserved in the Greenland Ice Sheet at summit; environmental implications. *Geophys. Res. Lett.* **21**, 693–696 (1994).
56. D. R. Marchant, G. H. Denton, C. C. Swisher, N. Potter, Late cenozoic antarctic paleoclimate reconstructed from volcanic ashes in the Dry Valleys region of southern Victoria Land. *Geol. Soc. Am. Bull.* **108**, 181–194 (1996).